Atmospheric
Chemistry
and Physics
Discussions

Open Access

Tropospheric carbon monoxide over the Pacific during HIPPO: two-way coupled simulation of GEOS-Chem and its multiple nested models

Y.-Y. Yan, J.-T. Lin, Y. Kuang, D. Yang, and L. Zhang

Laboratory for Climate and Ocean-Atmosphere Studies, Department of Atmospheric and Oceanic Sciences, School of Physics, Peking University, Beijing 100871, China

Correspondence to: J.-T. Lin (linjt@pku.edu.cn)

Title Page

Abstract	Introduction
Conclusions	References
Tables	Figures

|◀ | ▶|

◀ | ▶

Back | Close

Full Screen / Esc

Printer-friendly Version

Interactive Discussion

Abstract

Global chemical transport models (CTMs) are used extensively to study air pollution and transport at a global scale. These models are limited by coarse horizontal resolutions, not allowing for detailed representation of small-scale nonlinear processes over the pollutant source regions. Here we couple the global GEOS-Chem CTM and its three high-resolution nested models to simulate the tropospheric carbon monoxide (CO) over the Pacific Ocean during five HIAPER Pole-to-Pole Observations (HIPPO) campaigns between 2009 and 2011. We develop a two-way coupler, PKUCPL, to integrate simulation results for chemical constituents from the global model (at 2.5° long. × 2° lat.) and the three nested models (at 0.667° long. × 0.5° lat.) covering Asia, North America and Europe, respectively. The coupler obtains nested model results to modify the global model simulation within the respective nested domains, and simultaneously acquires global model results to provide lateral boundary conditions for the nested models.

Compared to the global model alone, the two-way coupled simulation results in enhanced CO concentrations in the nested domains. Sensitivity tests suggest the enhancement to be a result of improved representation of the spatial distributions of CO, nitrogen oxides and non-methane volatile organic compounds, the meteorological dependence of natural emissions, and other resolution-dependent processes. The relatively long lifetime of CO allows for the enhancement to be accumulated and carried across the globe. We find that the two-way coupled simulation increases the global tropospheric mean CO concentrations in 2009 by 10.4 %, with a greater enhancement at 13.3 % in the Northern Hemisphere. Coincidently, the global tropospheric mean hydroxyl radical (OH) is reduced by 4.2 % (as compared to the interannual variability of OH at 2.3 %), resulting in a 4.2 % enhancement in the methyl chloroform lifetime (MCF, via reaction with tropospheric OH). The resulting CO and OH contents and MCF lifetime are closer to observation-based estimates.

Both the global and the two-way coupled models capture the general spatiotemporal patterns of HIPPO CO over the Pacific. The two-way coupled simulation is much closer

to HIPPO CO, with a mean bias of 1.1 ppb (1.4 %) below 9 km compared to the bias at −7.2 ppb (−9.2 %) for the global model. The improvement is most apparent over the North Pacific. Our test simulations show that the global model could resemble the two-way coupled simulation (especially below 4 km) by increasing its global CO emissions by 15 % for HIPPO-1 and HIPPO-3, by 25 % for HIPPO-2 and HIPPO-4, and by 35 % for HIPPO-5. This has important implications for using the global model to constrain CO emissions. Thus, the two-way coupled simulation is a significantly improved model tool to studying the global impacts of air pollutants from major anthropogenic source regions.

1 Introduction

Global air pollution and transport is of interest worldwide, concerning the impacts on atmospheric chemistry, environment, and climate (Akimoto, 2003; Fiore et al., 2009; HTAP, 2010; Guan et al., 2014; Lin et al., 2014). Atmospheric transport across the Pacific Ocean is studied extensively due to concerns on air quality over North America (Wuebbles et al., 2007; Lin et al., 2008a, 2014; Zhang et al., 2008; Cooper et al., 2010; Yu et al., 2012). Carbon monoxide (CO) is used often as a transport tracer because of its relatively long lifetime in the troposphere (1–3 months) (Liu et al., 2003, 2013; Liang et al., 2004; Zhang et al., 2008). Transport of CO and other pollutants to the Pacific Ocean is measured often by aircraft campaigns and satellite remote sensing (Liu et al., 2003; Zhang et al., 2008). The recent five HIAPER Pole-to-Pole Observations (HIPPO) campaigns measured various atmospheric constituents over the Pacific from 2009 to 2011 (Wofsy, 2011) (see Fig. 1 for flight tracks and times). They provide detailed information on the seasonal and vertical structures of CO over the Pacific (Kort et al., 2012), ideal for studying its spatiotemporal variability and for source attribution.

Analyses of global air pollution and transport are facilitated often by global chemical transport models (CTMs) that simulate various chemical, physical and transport processes affecting air pollutants in the troposphere (Wild and Akimoto, 2001; Lin et al.,

2008b, 2014; Zhang et al., 2008; Fiore et al., 2009; Liu et al., 2013). Global CTMs normally have a horizontal resolution of 200–500 km (Fiore et al., 2009; Lamarque et al., 2013), not able to capture nonlinear processes at various fine scales over the pollutant source regions. Over the past decades, nested CTMs with much increased horizontal resolutions have been developed by the global CTM community (e.g., GEOS-Chem (Chen et al., 2009) and TM5, Krol et al., 2005) to better study air pollution characteristics over major pollutant source regions. For similar purposes, regional air quality models such as AQM, CMAQ and WAF-Chem have also been established with high horizontal resolutions (Huang et al., 2008; Lam and Fu, 2009; Pfister et al., 2011). These regional or nested models often obtain lateral boundary conditions (LBCs) of chemicals from global CTM simulations, and they capture many small-scale processes under-represented by global CTMs. However, the high-resolution simulation results are rarely used for feedback to improve global CTM simulations. Such "one-way" combination of global and regional models does not allow for high-resolution regional models to help study the global air pollutant transport.

In this paper, we use the GEOS-Chem CTM simulations to analyze the tropospheric CO over the Pacific Ocean measured from the five HIPPO campaigns over 2009–2011. For this purpose, we develop a two-way coupler, PeKing University CouPLer (PKUCPL), to integrate results of the global GEOS-Chem model (at $2.5°$ long. $\times 2°$ lat.) and its three nested models (at $0.667°$ long. $\times 0.5°$ lat.). These nested models cover Asia (Chen et al., 2009), North America (Zhang et al., 2011) and Europe (Vinken et al., 2014), respectively. The coupler acquires nested model results to replace global model results within the respective nested domains, in addition to letting the global CTM provide LBCs to the nested models. The coupler minimizes the computational cost of two-way integration by allowing the four models to run parallel to each other.

The rest of the paper is organized as follows. Section 2 describes the four GEOS-Chem models together with the two-way coupling framework. Section 3 presents an overall analysis of tropospheric CO simulated by the global CTM alone and by the two-way coupled model. Section 4 analyzes the tropospheric CO over the Pacific during the

HIPPO campaigns, evaluating simulation results from the global model and the two-way coupled model. The analysis is focused on the seasonal and vertical variability of CO, with important implications found for using the coarse-resolution global model to constrain CO emissions. Section 5 concludes the present study.

2   GEOS-Chem and the two-way coupling framework

2.1   GEOS-Chem models

Both the global and three nested GEOS-Chem CTMs (version 08-03-02; http://wiki.seas.harvard.edu/geos-chem/index.php/Main_Page) are driven by the GEOS-5 assimilated meteorological data from the National Aeronautic and Space Administration Global Modeling and Assimilation Office. The nested models are run at a horizontal resolution of $0.667°$ long. $\times$ $0.5°$ lat. native to the GEOS-5 data (see Fig. 2a for nested domains). The global model is run at a reduced resolution of $2.5°$ long. $\times$ $2°$ lat. with meteorological data regridded from the high-resolution GEOS-5 data. All models have 47 vertical layers.

All models are run with the full O_x-NO_x-VOC-CO-HO_x gaseous chemistry with online aerosol calculations. Model convection follows a modified Relaxed Arakawa–Schubert scheme (Rienecker et al., 2008). Vertical mixing in the planetary boundary layer is parameterized with a non-local scheme (Holtslag and Boville, 1993; Lin and McElroy, 2010).

Global anthropogenic emissions of nitrogen oxides (NO_x), CO and non-methane volatile organic compounds (NMVOC) are taken from the EDGAR 3.2-FT2000 dataset (Olivier et al., 2005). Emissions over Asia, North America and Europe are further replaced by various regional inventories shown in Table 1. Emission data are available at $1°$ long. $\times$ $1°$ lat. or finer resolutions, and are regridded to model resolutions prior to the simulation of photochemistry. No interannual variability is imposed. Over Asia, temperature dependence is imposed upon residential emissions (Streets, 2003; Lin,

2012). Figure 3a shows that global annual anthropogenic emissions of CO amount to to about $590 \, \text{Tg yr}^{-1}$ with weak seasonality below 20 %.

Monthly biomass burning emissions are taken from the GFED2 dataset (van der Werf et al., 2006), with CO emissions updated to GFED3.1 (van der Werf et al., 2010). Figure 3b shows that global monthly biomass burning emissions of CO vary between 6.3 and $96 \, \text{Tg month}^{-1}$ over the course of 2008–2011, depending on the climatic conditions. Over the nested domains (Fig. 3b), biomass burning emissions of CO vary more drastically with time.

Other emissions are calculated online, which is dependent of model meteorology and resolution. Lightning emissions of NO_x are parameterized based on cloud heights (Price et al., 1997), with a local adjustment based on the OTD/LIS satellite measurements (Sauvage et al., 2007; Murray et al., 2013) and a backward "C-shape" vertical profile (Ott et al., 2010). Soil emissions of NO_x follow Yienger and Levy (1995) and Wang et al. (1998). Biogenic emissions of NMVOC follow MEGAN v2.1 (Guenther et al., 2006).

For 2009, global emissions from all sources used in the coarse-resolution global model are about $45 \, \text{Tg N yr}^{-1}$ for NO_x and $587 \, \text{Tg C yr}^{-1}$ for NMVOC. Due to the resolution-dependent online calculation of biogenic NMVOC emissions and soil and lightning NO_x emissions, the global all-source emissions in the two-way coupled model are larger than those in the global model by 5 % for NMVOC and by 1 % for NO_x.

Figure 3c presents illustrative horizontal distributions of emissions over eastern China (part of the Asian nested domain). It shows that the spatial variability of emissions are much better resolved on the nested grid than on the global grid. As detailed in Sect. 3.2, better resolved emissions contribute to a significantly improved simulation of CO.

Simulations of both the global model and the two-way coupled model are conducted from July 2008 through 2011 to analyze the tropospheric CO during the HIPPO campaigns. Initial conditions of chemicals are regridded from a simulation at 5° long. × 4° lat. conducted from 2005. Simulations over July–December 2008 allow for a 6 month

Title Page

Abstract	Introduction
Conclusions	References
Tables	Figures

|◄ | ►|

◄ | ►

Back | Close

Full Screen / Esc

Printer-friendly Version

Interactive Discussion

spin-up for our focused analysis over 2009–2011. Ancillary test simulations are also performed over shorter periods (from July 2008 to January or to December 2009) to elaborate the physical mechanisms affecting the CO simulation under the two-way coupling framework.

2.2 Two-way coupling setup

Figure 4 shows the flowchart to couple the global and nested models. All models are regulated by the PKUCPL coupler. The coupler determines when and how to output global model results to update the LBCs of nested models, and to output nested model results to adjust the global model. Information of all chemical species is exchanged every three hours between the global and nested models. At the time step for information exchange, the propagation of a particular model is paused until all relevant information has been updated.

Figure 2b illustrates the global and nested model grid cells for information exchange. For a nested model, a buffer zone consisting of three nested grid cells is implemented on each edge of the nested domain (Fig. 2b). At the time to update LBCs, mixing ratios of all chemical species in the buffer zone are taken directly from the respectively grid cells of the global model. A more detailed description of the LBC setups can be found in Chen et al. (2009). While providing the LBCs, global model results in the troposphere are replaced by nested model results within the respective nested domains. Specifically, mass concentrations of all chemical species are outputted from nested models, regridded horizontally to match the global model grid with mass conservation guaranteed, and then used to replace global model results in the troposphere. Global model grid cells overlapping with the buffer zone of a nested model are not adjusted (Fig. 2b).

Under the two-way coupling framework, all models proceed in parallel. The computational time of the coupled system is greater than the slowest individual model (the nested model for North America) by 10 % only; the additional time is used for information exchange between models. With 8-core (Intel(R) Xeon(R) CPU X7550 @ 2.00 GHz)

OpenMP parallelization for each global or nested model, the coupled system takes about 10 days to finish one simulation year.

2.3 Testing the accuracy of the two-way coupling

Several issues warrant considerations for the two-way coupling. First, the coupled simulation may be affected by the frequency of inter-model data exchange. We find that increasing the exchange frequency from every three hours to every one hour does not affect the CO simulation after the 6 month spin-up period.

In addition, our treatment of LBCs is relatively simplified as the horizontal fluxes of chemicals (Krol et al., 2005) are not accounted for explicitly. This introduces certain random perturbations to the nested models that might in turn affect the global simulation in the two-way coupled system. We thus conduct a test two-way coupled simulation that successively increases the LBCs by 5 % for all chemical species at an exchange time step and then decreases the LBCs by 5 % at the next time step. We find that, even with such a large perturbation, the test simulation reproduces the two-way coupled simulation without the 5 % perturbation after the 6 month spin-up period.

Furthermore, mass conservation is required in regridding the nested model results to modify the global model. To address the mass conservation issue, we conduct additional test simulations by turning off all source and sink processes in both the global model and the two-way coupled model. Since the two simulations use the same initial conditions and only simulate the transport processes, mass conservation means that the total atmospheric content of CO should be the same between the global model and the two-way coupled model. Indeed, the test two-way coupled simulation reproduces the CO content simulated by the test global model.

Two-way coupled simulation of GEOS-Chem

Y.-Y. Yan et al.

Title Page

Abstract | Introduction

Conclusions | References

Tables | Figures

◀ | ▶

◀ | ▶

Back | Close

Full Screen / Esc

Printer-friendly Version

Interactive Discussion

3   General comparisons of tropospheric CO and hydroxyl radical simulated by the two-way coupled model vs. the global model

Figure 5 compares the day-to-day variations of tropospheric mean CO mixing ratios from July 2008 through December 2009 simulated by the global model (black lines) vs. the two-way coupled model (red lines). The spin-up period of July–December 2008 is included to elaborate the propagation differentiating the global model simulation from the two-way coupled simulation. In the three nested domains (Fig. 5b–d), the tropospheric mean CO simulated by the global model varies from 70 ppb to 115 ppb over the 1.5 years. CO reaches a maximum in the Northern Hemisphere winter-spring with a minimum in summer, reflecting the seasonal variation in CO sources and lifetime (Liang et al., 2004). The two-way coupled model produces more CO than the global model; the difference in 2009 is about 12.9 ppb (13.9 %) averaged over Asia, 8.9 ppb (11.2 %) over North America, and 9.4 ppb (11.7 %) over Europe.

Globally (Fig. 5a), CO mixing ratios in 2009 simulated by the two-way coupled model is about 7.4 ppb (10.4 %) higher than those simulated by the global model alone. The enhancement is more significant in the Northern Hemisphere (13.3 %); this alleviates the negative bias over the Northern Hemisphere typical for coarse-resolution global models (Naik et al., 2013). The enhancement is smaller in the Southern Hemisphere (6.9 %).

Table 2 further shows the CO budget in 2009. The tropospheric CO loss simulated by the two-way coupled model is close to that simulated by the global model. This is due to the decrease in OH content (see Sect. 3.3) compensating for the enhancement in CO. However, the mean tropospheric lifetime of CO (burden divided by loss) is enhanced by 9.0 %, from 1.75 months to 1.91 months.

3.1 Propagation differentiating the two-way coupled simulation from the global model

To elucidate how the difference between the two-way coupled model and the global model accumulates, we also conduct simulations with one-way nested models (i.e., no feedbacks to the global model; blue lines in Fig. 5b–d). CO concentrations simulated by the one-way nested models differ slightly from global model results on any given day, but the difference varies from one day to another (as evident from the green lines). On average, the one-way nested models produce daily mean CO higher than the global model by 1.24 ppb over Asia and 0.68 ppb over North America and lower by 0.15 ppb over Europe. Here, the nested models adopt LBCs from the global model every three hours with no influences on the global model, thus the CO difference cannot be accumulated effectively throughout time. With the two-way coupling (red lines), however, these regional differences are used to modify the global model every three hours and, with the long lifetime of CO, are accumulated and carried across the globe.

Figure 5d shows that over Europe, the one-way nested model (blue line) results in lower CO than the global model (black line), while the two-way coupled model (red line) produces higher CO than the global model. This is due to elevated transport of CO produced in Asia and North America via the two-way coupling mechanism. Such interaction between high-resolution simulations in multiple regions was unexplored previously and warrant further research.

3.2 Factors differentiating the two-way coupled model from the global model

Table 3 identifies various factors differentiating the two-way coupled model from the global model, taking the simulated CO in January 2009 for analysis. In January 2009, the global tropospheric mean CO simulated by the two-way coupled model is larger than that simulated by the global model by 9.6 %. Various test simulations are conducted from July 2008 through January 2009 to help delineate the differentiating fac-

Title Page

Abstract | Introduction

Conclusions | References

Tables | Figures

|◄ | ►|

◄ | ►

Back | Close

Full Screen / Esc

Printer-friendly Version

Interactive Discussion

tors. As shown below, the contributions of these factors are derived in a linear manner as a first-order estimate.

First, the magnitude of emissions differs between the two simulations. As shown in Sect. 2.1, global all-source emissions are larger in the two-way coupled model than in the global model by 5% for NMVOC and by 1% for NO_x. The additional NMVOC emissions increase the tropospheric CO, whereas the extra NO_x emissions have a negative impact on CO (by increasing the OH content). A test simulation with the global model adopts all emissions in the nested domains from the two-way coupled model at every time step, via a mass-conserved grid-conversion process. The test simulation increases the tropospheric CO in January 2009 by 3.5% compared to the standard global model (Table 3), roughly representing the effect of differences in emission magnitude between the two-way coupled model and the global model. The residual difference of 6.1% (i.e., 9.6% minus 3.5%) represents the combined effect of all factors other than emission magnitude.

Furthermore, the two-way coupled model better captures the small-scale spatial variability of NO_x, NMVOC and CO concentrations in the nested domains with a consequence on the photochemical efficiency. Such variability in concentration is driven by the variability in emissions (see Fig. 3c for example), since the two-way coupled model use the same initial conditions as the global model. To derive the effect of small-scale emission variability, we conduct a test simulation of the two-way coupled model by adopting all emissions from the global model at every time step. Here, emissions are regridded from $2.5°$ long. $\times 2°$ lat. to $0.667°$ long. $\times 0.5°$ lat. in the nested domains such that horizontal variability at scales smaller than $2.5°$ long. $\times 2°$ lat. are not resolved. As a result, the test two-way coupled simulation produces higher CO by 1.5% than the standard global model in January 2009. The 1.5% difference represents the combined effect of non-emission small-scale variability (related to vertical transport, radiation, and other resolution-dependent processes) that is resolved on the $0.667°$ long. $\times 0.5°$ lat. grid but not on the $2.5°$ long. $\times 2°$ lat. grid. Therefore, the effect of small-scale variability in NO_x, NMVOC and CO concentrations/emissions is estimated at 4.6% (i.e., 6.1%

minus 1.5 %), contributing about half of the difference between the two-way coupled model and the global model.

3.3 Impacts on tropospheric OH abundance and methyl chloroform lifetime

Table 4 shows the impacts of two-way coupling on the tropospheric OH budget. Consistent with the increased CO content, the air mass weighted global mean tropospheric OH in 2009 simulated by the two-way coupled model is lower than that simulated by the global model by 4.2 % (11.9×10^5 vs. 12.4×10^5 molec cm^{-3}). The 4.2 % difference exceeds the standard deviation of OH interannual variation estimated at 2.3 % (Montzka et al., 2011). The OH reduction is more significant in the Northern Hemisphere (5.7 %) than in the Southern Hemisphere (2.1 %), reducing the northern/southern hemispheric OH ratio from 1.27 to 1.24. This change helps alleviate the overestimate in hemispheric OH contrast typical for coarse-resolution global CTMs (Naik et al., 2013). The production and loss rates of OH are affected insignificantly, however (Table 4). For example, the loss via OH + CO reaction changes marginally due to the increased CO concentration compensating for the decreased OH.

The reduced OH abundance leads to an enhanced lifetime of methyl chloroform via tropospheric OH from 5.3 yr to 5.5 yr, a 4.2 % increase. The enhanced lifetime is closer to the observation-based estimate at 6.0–6.3 yr (Prinn et al., 2005; Prather et al., 2012).

4 Evaluation of simulated CO over the Pacific during the five HIPPO campaigns

4.1 Selection of HIPPO CO data and coincident model results

Figure 1 shows the flight tracks and dates of five HIPPO aircraft campaigns conducted in various seasons between 2009 and 2011. These campaigns were designed to measure atmospheric trace constituents in the remote troposphere over the Pacific, Arctic, and near-Antarctic regions (Wofsy, 2011). In these campaigns, aircrafts took off in central North America, flied northward to almost 85° N, turned southward until 75° S, and

finally went back to North America. The measurements provide a large quantity of global-scale high-quality data for analysis of atmospheric chemistry in these remote areas.

During HIPPO, CO was measured by direct absorption spectroscopy using the Harvard University/Aerodyne Research Quantum Cascade Laser Spectrometer (Jimenez et al., 2005; Kort et al., 2012). To evaluate GEOS-Chem simulations, this study uses the merged dataset providing the tropospheric CO mixing ratios at a vertical resolution of 0.1 km (see http://hippo.ornl.gov/node/16). A total of 620 vertical profiles over the Pacific Ocean are employed, with 124 profiles from HIPPO-1, 98 from HIPPO-2, 103 from HIPPO-3, 143 from HIPPO-4, and 152 from HIPPO-5. Model CO are sampled at the times and locations of individual measurements to ensure spatiotemporal consistency with the HIPPO data.

4.2 General spatiotemporal pattern of the Pacific CO during HIPPO

Figure 6a shows the time-height distribution of CO mixing ratios over the Pacific measured from the five campaigns. Most measurements are concentrated below 10 km, especially below 9 km. Below 10 km, CO normally exceed 80 ppb at the beginning and end of each campaign measured over the North Pacific, with values normally lower than 70 ppb in between measured over the South Pacific (Wofsy, 2011). The hemispheric contrast is due mainly to the larger sources of CO in the Northern Hemisphere.

Figure 6a shows that the measured North Pacific CO mixing ratios reach a maximum during HIPPO-3 in March–April 2010. This reflects in part the strong Asian biomass burning emissions in the period (Fig. 3b). Asian influences are also enhanced in spring because of increased midlatitude cyclonic activities supplemented by a relatively long lifetime of CO (Liu et al., 2003; Liang et al., 2004). By comparison, the North Pacific CO mixing ratios are lowest during HIPPO-4 and HIPPO-5 over June-September 2011 when the lifetime of CO reaches a minimum (Liang et al., 2004).

Figure 6b and c shows that both the global model and the two-way coupled model reproduce the general spatiotemporal structure of HIPPO CO. However, the two-way

coupled simulation is closer to HIPPO CO than the global model, particularly for the high values over the North Pacific. The global model generally underestimates HIPPO CO with a mean bias by -7.2 ppb (-9.2 %) below 9 km; the bias is much larger over the North Pacific (-10.2 ppb, -13.1 %) than over the South Pacific (-1.6 ppb, -2.1 %). This is consistent with the negative bias in the Northern Hemisphere typical for coarse-resolution global CTMs (Naik et al., 2013).

Figure 7 further evaluates the simulated CO mixing ratios in each vertical layer of 1 km thick (Layer 1 for 0–1 km, Layer 2 for 1–2 km, etc.) during the five HIPPO campaigns. Compared to the global model, the two-way coupled simulation reduces the mean normalized bias relative to HIPPO CO in all but the 10th, 11th and 12th layers (between 9 km and 12 km). Note that comparisons at higher altitudes, especially above 10 km, are subject to scarcity in measurements (Fig. 6a). In all layers, the two-way coupled model also slightly improves the correlation with HIPPO CO.

4.3 Vertical profile of the Pacific CO during HIPPO

The thick yellow lines in Fig. 8a–e shows the mean vertical distributions of CO measured from individual HIPPO campaigns. In general, the measured CO mixing ratios are larger in the lower and middle troposphere than in the upper troposphere. The largest vertical contrast occurs during HIPPO-3 in March–April 2010, with CO reaching 105 ppb near the surface and at around 5–6 km in contrast to a value of 60 ppb at 12 km. The vertical contrast reflects the strong springtime Asian outflow in the lower and middle troposphere (Liu et al., 2003; Liang et al., 2004). By comparison, the vertical contrast is only about 10 ppb during HIPPO-4 in June–July 2011, due to strong convective activities in the Northern Hemisphere summer that mix CO more evenly. During HIPPO-5 in August–September 2011, CO mixing ratios change by 20 ppb at around 9 km due to the stratospheric influences, as shown also in model simulations.

The red lines in Fig. 8a–e shows that the two-way coupled simulation captures the vertical distribution of HIPPO CO. The bias is smallest during HIPPO-1 where the model reproduces various fine structures of HIPPO CO throughout the troposphere

(Fig. 8a). Averaged across the five campaigns (Fig. 8f), the two-way coupled simulation is within 3 ppb of HIPPO CO below 9 km with an overestimate by 1–5 ppb above 9 km; the mean bias is 1.1 ppb (1.4 %) for 0–9 km and 2.1 ppb (3.1 %) for 0–13 km. The global model also captures the general vertical structure of HIPPO CO, but with negative biases during all campaigns (Fig. 8a–e, black lines). Averaged across the five campaigns (Fig. 8f), the global model underestimates the HIPPO CO by 1–10 ppb throughout the troposphere; the mean bias reaches −6.2 ppb (−8.3 %) for 0–13 km and −7.2 ppb (−9.2 %) for 0–9 km.

4.4 Implications of model resolution dependence for CO emission constraint

The global model is used often to constrain CO emissions, where the mean model bias relative to measurements is attributed to emission errors (Stavrakou and Müller, 2006; Kopacz et al., 2010; Hooghiemstra et al., 2011). Previous studies have discussed uncertainties in model transport (Liu et al., 2010; Jiang et al., 2013) and the OH field (Kopacz et al., 2010; Hooghiemstra et al., 2011) affecting emission constraints. Here we show that the tropospheric CO simulated by the two-way coupled model are much higher than the global model and are much closer to HIPPO measurements, as a consequence of improved representation of resolution-dependent emissions, chemistry, physics, and transport. This has important implications for using the global model to constrain CO emissions.

To elaborate this point, we adjust CO emissions in the global model in an attempt to reproduce the two-way coupled simulation. We find that the global model simulation can resemble the two-way coupled simulation during HIPPO-1, especially below 4 km, by increasing global CO emissions from all sources by 15 % (Fig. 8a, green line). Emission increases with respect to other campaigns are 25 % for HIPPO-2, 15 % for HIPPO-3, 25 % for HIPPO-4, and 35 % for HIPPO-5 (Fig. 8b–e, green lines). Here all simulations start from July 2008 with adjusted CO emissions. The extent of required emission increases is larger than the magnitude of CO difference (about 11 % based on Sects. 4.2 and 4.3), because emissions contribute less than half of tropospheric CO

sources. As shown in Table 2, emissions contribute about 38 % of tropospheric CO in 2009, with the residual 62 % attributed to oxidation of methane and NMVOC. The simulation results here imply that, when used for emission constraints, the two-way coupled simulation would suggest much lower CO emissions to match measurements than the coarse-resolution global model.

5 Conclusions

We develop a two-way coupler, PKUCPL, to integrate the global GEOS-Chem CTM (at 2.5° long. × 2° lat.) and its three high-resolution nested models (at 0.667° long. × 0.5° lat.) covering Asia, North America and Europe, respectively. Under the coupling framework, the global model provides LBCs of chemicals for the nested models, while the nested models produce high-resolution results to improve the global model within the respective nested domains. The nested models encompass major anthropogenic pollutant source regions and better capture many small-scale nonlinear processes underrepresented by the global model; and the two-way coupling allows for such improvements to have a global impact.

Analysis for 2009 show that the tropospheric CO simulated by the two-way coupled model are much higher than those simulated the global model, with a difference by 10.4 % averaged across the globe. The enhancement reaches 13.3 % in the Northern Hemisphere, alleviating the northern hemispheric underestimate typical for global models (Naik et al., 2013). The increase in CO is accompanied by a 4.2 % reduction in global mean tropospheric mean OH, the magnitude of which is larger than the OH interannual variability estimated at 2.3 % (Montzka et al., 2011). The reduction in OH content results in a 4.2 % enhancement (from 5.3 years to 5.5 years) in the methyl chloroform lifetime via reaction with tropospheric OH, bringing it closer to observation-based estimates at 6.0–6.3 yr (Prinn et al., 2005; Prather et al., 2012).

We delineate the factors differentiating the two-way coupled model from the global model in a simplified linear manner, taking for illustration the simulated CO concentra-

Title Page

Abstract | Introduction

Conclusions | References

Tables | Figures

|◄ | ►|

◄ | ►

Back | Close

Full Screen / Esc

Printer-friendly Version

Interactive Discussion

tion in January 2009. The two-way coupled simulation results in higher CO by 9.6 % in January 2009. We find that a 4.6 % enhancement is due to improved representation of small-scale spatial variability in NO_x, NMVOC and CO resolved on the fine grid but not on the coarse grid. Another 3.5 % enhancement is due to increased soil and lightning emissions of NO_x and especially biogenic emissions of NMVOC that are dependent of model meteorology and resolution. And an additional 1.5 % enhancement is due to improved simulation of vertical transport, radiation, and other resolution-dependent processes.

We use the two-way coupled model and the global model to simulate the tropospheric CO mixing ratios over the Pacific during the five HIPPO campaigns in various seasons between 2009 and 2011. Both models capture the general seasonal, horizontal and vertical distributions of HIPPO CO. Compared to the global model, the two-way coupled model correlates better with HIPPO CO spatiotemporally. Averaged across the five campaigns, CO simulated by the two-way coupled model is within 3 ppb of HIPPO CO below 9 km with a positive bias by 1–5 ppb above 9 km; the mean bias is 1.1 ppb (1.4 %) for 0–9 km and 2.1 ppb (3.1 %) for 0–13 km. The global model underestimates HIPPO CO by 1–10 ppb throughout the troposphere with a mean bias by −6.2 ppb (−8.3 %); the bias is most apparent over the North Pacific, consistent with the northern hemispheric underestimate typical for global models (Naik et al., 2013).

Our test simulations with the global model suggest that increasing the global CO emissions from all sources by about 15 % would lead to CO mixing ratios comparable to those simulated by the two-way coupled model during HIPPO-1, especially below 4 km; the respective emission increases are 25 % for HIPPO-2, 15 % for HIPPO-3, 25 % for HIPPO-4, and 35 % for HIPPO-5. These results imply an important model dependence on horizontal resolution that is largely unaccounted for in the literature on CO emission constraints.

Our two-way coupling framework minimizes the computational time and model complexity concerned commonly for multi-model integration. This is achieved by running all models in parallel under the regulation of the master coupler PKUCPL. With this

Two-way coupled simulation of GEOS-Chem

Y.-Y. Yan et al.

Title Page

Abstract	Introduction
Conclusions	References
Tables	Figures

|◀ | ▶|

◀ | ▶

Back | Close

Full Screen / Esc

Printer-friendly Version

Interactive Discussion

coupler, it is straightforward to incorporate additional nested models with the same or different horizontal resolutions. In particular, a much finer nested GEOS-Chem model (at 0.3125° long. × 0.25° lat.) is currently available for North America and under development for other regions. As such, it is feasible to develop a low-computational-cost multi-regional multi-layer two-way coupling system to facilitate research on the interactions between global, regional and local scales. The coupled system will help address questions such as the impacts of megacities and urbanization on pollutant transport, global environment, and climate change (Parrish and Zhu, 2009).

References

Akimoto, H.: Global air quality and pollution, Science, 302, 1716–1719, 2003.

Auvray, M. and Bey, I.: Long-range transport to Europe: seasonal variations and implications for the European ozone budget, J. Geophys. Res.-Atmos., 110, D11303, doi:10.1029/2004jd005503, 2005.

Chen, D., Wang, Y., McElroy, M. B., He, K., Yantosca, R. M., and Le Sager, P.: Regional CO pollution and export in China simulated by the high-resolution nested-grid GEOS-Chem model, Atmos. Chem. Phys., 9, 3825–3839, doi:10.5194/acp-9-3825-2009, 2009.

Cooper, O. R., Parrish, D. D., Stohl, A., Trainer, M., Nedelec, P., Thouret, V., Cammas, J. P., Oltmans, S. J., Johnson, B. J., Tarasick, D., Leblanc, T., McDermid, I. S., Jaffe, D., Gao, R., Stith, J., Ryerson, T., Aikin, K., Campos, T., Weinheimer, A., and Avery, M. A.: Increasing springtime ozone mixing ratios in the free troposphere over western North America, Nature, 463, 344–348, doi:10.1038/nature08708, 2010.

Fiore, A. M., Dentener, F. J., Wild, O., Cuvelier, C., Schultz, M. G., Hess, P., Textor, C., Schulz, M., Doherty, R. M., Horowitz, L. W., MacKenzie, I. A., Sanderson, M. G., Shindell, D. T., Stevenson, D. S., Szopa, S., Van Dingenen, R., Zeng, G., Atherton, C., Bergmann, D., Bey, I., Carmichael, G., Collins, W. J., Duncan, B. N., Faluvegi, G., Fol-

berth, G., Gauss, M., Gong, S., Hauglustaine, D., Holloway, T., Isaksen, I. S. A., Jacob, D. J., Jonson, J. E., Kaminski, J. W., Keating, T. J., Lupu, A., Marmer, E., Montanaro, V., Park, R. J., Pitari, G., Pringle, K. J., Pyle, J. A., Schroeder, S., Vivanco, M. G., Wind, P., Wojcik, G., Wu, S., and Zuber, A.: Multimodel estimates of intercontinental source-receptor relationships for ozone pollution, J. Geophys. Res.-Atmos., 114, D04301, doi:10.1029/2008jd010816, 2009.

Guan, D.-B., Lin, J.-T., Davis, S. J., Pan, D., He, K.-B., Wang, C., Wuebbles, D. J., Streets, D. G., and Zhang, Q.: Response to Lopez et al.: Consumption-based accounting helps mitigate global air pollution, P. Natl. Acad. Sci. USA, doi:10.1073/pnas.1407383111, 2014.

Guenther, A., Karl, T., Harley, P., Wiedinmyer, C., Palmer, P. I., and Geron, C.: Estimates of global terrestrial isoprene emissions using MEGAN (Model of Emissions of Gases and Aerosols from Nature), Atmos. Chem. Phys., 6, 3181–3210, doi:10.5194/acp-6-3181-2006, 2006.

Holtslag, A. A. M. and Boville, B. A.: Local versus nonlocal boundary-layer diffusion in a global climate model, J. Climate, 6, 1825–1842, doi:10.1175/1520-0442(1993)006<1825:lvnbld>2.0.co;2, 1993.

Hooghiemstra, P. B., Krol, M. C., Meirink, J. F., Bergamaschi, P., van der Werf, G. R., Novelli, P. C., Aben, I., and Röckmann, T.: Optimizing global CO emission estimates using a four-dimensional variational data assimilation system and surface network observations, Atmos. Chem. Phys., 11, 4705–4723, doi:10.5194/acp-11-4705-2011, 2011.

HTAP: Hemispheric Transport of Air Pollution 2010 Executive SummaryECE/EB.AIR/2010/10 Corrected, United Nations, 2010.

Huang, H. C., Lin, J. T., Tao, Z. N., Choi, H., Patten, K., Kunkel, K., Xu, M., Zhu, J. H., Liang, X. Z., Williams, A., Caughey, M., Wuebbles, D. J., and Wang, J. L.: Impacts of long-range transport of global pollutants and precursor gases on US air quality under future climatic conditions, J. Geophys. Res.-Atmos., 113, D19307, doi:10.1029/2007jd009469, 2008.

Jiang, Z., Jones, D., Worden, H. M., Deeter, M. N., Henze, D. K., Worden, J., Bowman, K. W., Brenninkmeijer, C., and Schuck, T.: Impact of model errors in convective transport on CO source estimates inferred from MOPITT CO retrievals, J. Geophys. Res.-Atmos., 118, 2073–2083, 2013.

Jimenez, R., Herndon, S., Shorter, J. H., Nelson, D. D., McManus, J. B., and Zahniser, M. S.: Atmospheric trace gas measurements using a dual quantum-cascade laser mid-infrared ab-

sorption spectrometer, Proc.SPIE5738, Novel In-Plane Semiconductor Lasers IV, 318–331, doi:10.1117/12.597130, 2005.

Kopacz, M., Jacob, D. J., Fisher, J. A., Logan, J. A., Zhang, L., Megretskaia, I. A., Yantosca, R. M., Singh, K., Henze, D. K., Burrows, J. P., Buchwitz, M., Khlystova, I., McMillan, W. W., Gille, J. C., Edwards, D. P., Eldering, A., Thouret, V., and Nedelec, P.: Global estimates of CO sources with high resolution by adjoint inversion of multiple satellite datasets (MOPITT, AIRS, SCIAMACHY, TES), Atmos. Chem. Phys., 10, 855–876, doi:10.5194/acp-10-855-2010, 2010.

Kort, E. A., Wofsy, S. C., Daube, B. C., Diao, M., Elkins, J. W., Gao, R. S., Hintsa, E. J., Hurst, D. F., Jimenez, R., Moore, F. L., Spackman, J. R., and Zondlo, M. A.: Atmospheric observations of Arctic Ocean methane emissions up to 82 degrees north, Nat. Geosci., 5, 318–321, doi:10.1038/ngeo1452, 2012.

Krol, M., Houweling, S., Bregman, B., van den Broek, M., Segers, A., van Velthoven, P., Peters, W., Dentener, F., and Bergamaschi, P.: The two-way nested global chemistry-transport zoom model TM5: algorithm and applications, Atmos. Chem. Phys., 5, 417–432, doi:10.5194/acp-5-417-2005, 2005.

Kuhns, H., Etyemezian, V., Green, M., Hendrickson, K., McGown, M., Barton, K., and Pitchford, M.: Vehicle-based road dust emission measurement – Part II: Effect of precipitation, wintertime road sanding, and street sweepers on inferred PM_{10} emission potentials from paved and unpaved roads, Atmos. Environ., 37, 4573–4582, doi:10.1016/s1352-2310(03)00529-6, 2003.

Lam, Y. F. and Fu, J. S.: A novel downscaling technique for the linkage of global and regional air quality modeling, Atmos. Chem. Phys., 9, 9169–9185, doi:10.5194/acp-9-9169-2009, 2009.

Lamarque, J.-F., Shindell, D. T., Josse, B., Young, P. J., Cionni, I., Eyring, V., Bergmann, D., Cameron-Smith, P., Collins, W. J., Doherty, R., Dalsoren, S., Faluvegi, G., Folberth, G., Ghan, S. J., Horowitz, L. W., Lee, Y. H., MacKenzie, I. A., Nagashima, T., Naik, V., Plummer, D., Righi, M., Rumbold, S. T., Schulz, M., Skeie, R. B., Stevenson, D. S., Strode, S., Sudo, K., Szopa, S., Voulgarakis, A., and Zeng, G.: The Atmospheric Chemistry and Climate Model Intercomparison Project (ACCMIP): overview and description of models, simulations and climate diagnostics, Geosci. Model Dev., 6, 179–206, doi:10.5194/gmd-6-179-2013, 2013.

Liang, Q., Jaegle, L., Jaffe, D. A., Weiss-Penzias, P., Heckman, A., and Snow, J. A.: Long-range transport of Asian pollution to the northeast Pacific: seasonal variations

Title Page

Abstract | Introduction

Conclusions | References

Tables | Figures

|◄ | ►|

◄ | ►

Back | Close

Full Screen / Esc

Printer-friendly Version

Interactive Discussion

and transport pathways of carbon monoxide, J. Geophys. Res.-Atmos., 109, D23s07, doi:10.1029/2003jd004402, 2004.

Lin, J.-T.: Satellite constraint for emissions of nitrogen oxides from anthropogenic, lightning and soil sources over East China on a high-resolution grid, Atmos. Chem. Phys., 12, 2881–2898, doi:10.5194/acp-12-2881-2012, 2012.

Lin, J.-T. and McElroy, M. B.: Impacts of boundary layer mixing on pollutant vertical profiles in the lower troposphere: implications to satellite remote sensing, Atmos. Environ., 44, 1726–1739, doi:10.1016/j.atmosenv.2010.02.009, 2010.

Lin, J.-T., Wuebbles, D. J., and Liang, X. Z.: Effects of intercontinental transport on surface ozone over the United States: present and future assessment with a global model, Geophys. Res. Lett., 35, L02805, doi:10.1029/2007gl031415, 2008a.

Lin, J.-T., Youn, D., Liang, X., and Wuebbles, D.: Global model simulation of summertime U.S. ozone diurnal cycle and its sensitivity to PBL mixing, spatial resolution, and emissions, Atmos. Environ., 42, 8470–8483, doi:10.1016/j.atmosenv.2008.08.012, 2008b.

Lin, J.-T., Pan, D., Davis, S. J., Zhang, Q., He, K., Wang, C., Streets, D. G., Wuebbles, D. J., and Guan, D.: China's international trade and air pollution in the United States, P. Natl. Acad. Sci. USA, 111, 1736–1741, doi:10.1073/pnas.1312860111, 2014.

Liu, H. Y., Jacob, D. J., Bey, I., Yantosca, R. M., Duncan, B. N., and Sachse, G. W.: Transport pathways for Asian pollution outflow over the Pacific: interannual and seasonal variations, J. Geophys. Res.-Atmos., 108, 8786–8800, doi:10.1029/2002jd003102, 2003.

Liu, J., Logan, J. A., Murray, L. T., Pumphrey, H. C., Schwartz, M. J., and Megretskaia, I. A.: Transport analysis and source attribution of seasonal and interannual variability of CO in the tropical upper troposphere and lower stratosphere, Atmos. Chem. Phys., 13, 129–146, doi:10.5194/acp-13-129-2013, 2013.

Junhua Liu, Logan, J. A., Jones, D. B. A., Livesey, N. J., Megretskaia, I., Carouge, C., and Nedelec, P.: Analysis of CO in the tropical troposphere using Aura satellite data and the GEOS-Chem model: insights into transport characteristics of the GEOS meteorological products, Atmos. Chem. Phys., 10, 12207–12232, doi:10.5194/acp-10-12207-2010, 2010.

Montzka, S. A., Krol, M., Dlugokencky, E., Hall, B., Jockel, P., and Lelieveld, J.: Small interannual variability of global atmospheric hydroxyl, Science, 331, 67–69, doi:10.1126/science.1197640, 2011.

Murray, L. T., Logan, J. A., and Jacob, D. J.: Interannual variability in tropical tropospheric ozone and OH: the role of lightning, J. Geophys. Res.-Atmos., 118, 11468–11480, 2013.

Naik, V., Voulgarakis, A., Fiore, A. M., Horowitz, L. W., Lamarque, J.-F., Lin, M., Prather, M. J., Young, P. J., Bergmann, D., Cameron-Smith, P. J., Cionni, I., Collins, W. J., Dalsøren, S. B., Doherty, R., Eyring, V., Faluvegi, G., Folberth, G. A., Josse, B., Lee, Y. H., MacKenzie, I. A., Nagashima, T., van Noije, T. P. C., Plummer, D. A., Righi, M., Rumbold, S. T., Skeie, R., Shindell, D. T., Stevenson, D. S., Strode, S., Sudo, K., Szopa, S., and Zeng, G.: Preindustrial to present-day changes in tropospheric hydroxyl radical and methane lifetime from the Atmospheric Chemistry and Climate Model Intercomparison Project (ACCMIP), Atmos. Chem. Phys., 13, 5277–5298, doi:10.5194/acp-13-5277-2013, 2013.

Olivier, J. G., Van Aardenne, J. A., Dentener, F. J., Pagliari, V., Ganzeveld, L. N., and Peters, J. A.: Recent trends in global greenhouse gas emissions: regional trends 1970–2000 and spatial distributionof key sources in 2000, Environm. Sci., 2, 81–99, 2005.

Ott, L. E., Pickering, K. E., Stenchikov, G. L., Allen, D. J., DeCaria, A. J., Ridley, B., Lin, R.-F., Lang, S., and Tao, W.-K.: Production of lightning NO(x) and its vertical distribution calculated from three-dimensional cloud-scale chemical transport model simulations, J. Geophys. Res.-Atmos., 115, D04301, doi:10.1029/2009jd011880, 2010.

Parrish, D. D. and Zhu, T.: Clean air for megacities, Science, 326, 674–675, 2009.

Pfister, G. G., Parrish, D. D., Worden, H., Emmons, L. K., Edwards, D. P., Wiedinmyer, C., Diskin, G. S., Huey, G., Oltmans, S. J., Thouret, V., Weinheimer, A., and Wisthaler, A.: Characterizing summertime chemical boundary conditions for airmasses entering the US West Coast, Atmos. Chem. Phys., 11, 1769–1790, doi:10.5194/acp-11-1769-2011, 2011.

Prather, M. J., Holmes, C. D., and Hsu, J.: Reactive greenhouse gas scenarios: systematic exploration of uncertainties and the role of atmospheric chemistry, Geophys. Res. Lett., 39, L09803, doi:10.1029/2012GL051440, 2012.

Price, C., Penner, J., and Prather, M.: NO$_x$ from lightning. 1. Global distribution based on lightning physics, J. Geophys. Res.-Atmos., 102, 5929–5941, doi:10.1029/96jd03504, 1997.

Prinn, R., Huang, J., Weiss, R., Cunnold, D., Fraser, P., Simmonds, P., McCulloch, A., Harth, C., Reimann, S., and Salameh, P.: Evidence for variability of atmospheric hydroxyl radicals over the past quarter century, Geophys. Res. Lett., 32, L07809, doi:10.1029/2004GL022228, 2005.

Rienecker, E., Ryan, J., Blum, M., Dietz, C., Coletti, L., Marin III, R., and Bissett, W. P.: Mapping phytoplankton in situ using a laser-scattering sensor, Limnol. Oceanogr.-Meth., 6, 153–161, 2008.

Title Page

Abstract | Introduction

Conclusions | References

Tables | Figures

|◄ | ►|

◄ | ►

Back | Close

Full Screen / Esc

Printer-friendly Version

Interactive Discussion

Sauvage, B., Martin, R. V., van Donkelaar, A., Liu, X., Chance, K., Jaeglé, L., Palmer, P. I., Wu, S., and Fu, T.-M.: Remote sensed and in situ constraints on processes affecting tropical tropospheric ozone, Atmos. Chem. Phys., 7, 815–838, doi:10.5194/acp-7-815-2007, 2007.

Stavrakou, T. and Müller, J. F.: Grid-based versus big region approach for inverting CO emissions using Measurement of Pollution in the Troposphere (MOPITT) data, J. Geophys. Res.-Atmos. (1984–2012), 111, D15304, doi:10.1029/2005JD006896, 2006.

Streets, D. G.: An inventory of gaseous and primary aerosol emissions in Asia in the year 2000, J. Geophys. Res., 108, 8809, doi:10.1029/2002jd003093, 2003.

van der Werf, G. R., Randerson, J. T., Giglio, L., Collatz, G. J., Kasibhatla, P. S., and Arellano Jr., A. F.: Interannual variability in global biomass burning emissions from 1997 to 2004, Atmos. Chem. Phys., 6, 3423–3441, doi:10.5194/acp-6-3423-2006, 2006.

van der Werf, G. R., Randerson, J. T., Giglio, L., Collatz, G. J., Mu, M., Kasibhatla, P. S., Morton, D. C., DeFries, R. S., Jin, Y., and van Leeuwen, T. T.: Global fire emissions and the contribution of deforestation, savanna, forest, agricultural, and peat fires (1997–2009), Atmos. Chem. Phys., 10, 11707–11735, doi:10.5194/acp-10-11707-2010, 2010.

Vinken, G. C. M., Boersma, K. F., van Donkelaar, A., and Zhang, L.: Constraints on ship NO_x emissions in Europe using GEOS-Chem and OMI satellite NO_2 observations, Atmos. Chem. Phys., 14, 1353–1369, doi:10.5194/acp-14-1353-2014, 2014.

Wang, Y., Jacob, D. J., and Logan, J. A.: Global simulation of tropospheric O_3-NO_x-hydrocarbon chemistry, 1. Model formulation, J. Geophys. Res., 103, 10713–10725, doi:10.1029/98JD00158, 1998.

Wild, O. and Akimoto, H.: Intercontinental transport of ozone and its precursors in a three-dimensional global CTM, J. Geophys. Res.-Atmos., 106, 27729–27744, doi:10.1029/2000jd000123, 2001.

Wofsy, S. C.: HIAPER Pole-to-Pole Observations (HIPPO): fine-grained, global-scale measurements of climatically important atmospheric gases and aerosols, Philos. T. R. Soc. A, 369, 2073–2086, doi:10.1098/rsta.2010.0313, 2011.

Wuebbles, D. J., Lei, H., and Lin, J. T.: Intercontinental transport of aerosols and photochemical oxidants from Asia and its consequences, Environ. Pollut., 150, 65–84, doi:10.1016/j.envpol.2007.06.066, 2007.

Yienger, J. J. and Levy, H.: Empirical-model of global soil-biogenic NO_x emissions, J. Geophys. Res.-Atmos., 100, 11447–11464, doi:10.1029/95jd00370, 1995.

Title Page

Abstract | Introduction

Conclusions | References

Tables | Figures

|◄ | ►|

◄ | ►

Back | Close

Full Screen / Esc

Printer-friendly Version

Interactive Discussion

Yu, H., Remer, L. A., Chin, M., Bian, H., Tan, Q., Yuan, T., and Zhang, Y.: Aerosols from overseas rival domestic emissions over North America, Science, 337, 566–569, doi:10.1126/science.1217576, 2012.

Zhang, L., Jacob, D. J., Boersma, K. F., Jaffe, D. A., Olson, J. R., Bowman, K. W., Worden, J. R., Thompson, A. M., Avery, M. A., Cohen, R. C., Dibb, J. E., Flock, F. M., Fuelberg, H. E., Huey, L. G., McMillan, W. W., Singh, H. B., and Weinheimer, A. J.: Transpacific transport of ozone pollution and the effect of recent Asian emission increases on air quality in North America: an integrated analysis using satellite, aircraft, ozonesonde, and surface observations, Atmos. Chem. Phys., 8, 6117–6136, doi:10.5194/acp-8-6117-2008, 2008.

Zhang, L., Jacob, D. J., Downey, N. V., Wood, D. A., Blewitt, D., Carouge, C. C., van Donkelaar, A., Jones, D. B. A., Murray, L. T., and Wang, Y.: Improved estimate of the policy-relevant background ozone in the United States using the GEOS-Chem global model with $1/2° \times 2/3°$ horizontal resolution over North America, Atmos. Environ., 45, 6769–6776, doi:10.1016/j.atmosenv.2011.07.054, 2011.

Zhang, Q., Streets, D. G., Carmichael, G. R., He, K. B., Huo, H., Kannari, A., Klimont, Z., Park, I. S., Reddy, S., Fu, J. S., Chen, D., Duan, L., Lei, Y., Wang, L. T., and Yao, Z. L.: Asian emissions in 2006 for the NASA INTEX-B mission, Atmos. Chem. Phys., 9, 5131–5153, doi:10.5194/acp-9-5131-2009, 2009.

Title Page

Abstract | Introduction

Conclusions | References

Tables | Figures

|◄ | ►|

◄ | ►

Back | Close

Full Screen / Esc

Printer-friendly Version

Interactive Discussion

Table 1. Anthropogenic and biomass burning emission inventories used by GEOS-Chem.

Source type	Region	Dataset	Resolution[*]	References and Notes
Anthro.	Global	EDGAR 3.2-FT2000	1° long. × 1° lat.	Olivier et al. (2005)
	Asia	INTEX-B	0.5° long. × 0.5° lat.	Zhang et al. (2009)
	US	NEI05	4 km × 4 km	http://www.epa.gov/ttn/chief/net/2005 inventory.html#inventorydata Gridded data were adopted from WRF-Chem (ftp://aftp.fsl.noaa.gov/divisions/ taq/emissions_data_2005)
	Canada	CAC	1° long. × 1° lat.	http://www.ec.gc.ca/pdb/cac/cac_home_e.cfm
	Mexico	BRAVO	1° long. × 1° lat.	Kuhns et al. (2003)
	Europe	EMEP	0.5° long. × 0.5° lat.	Auvray and Bey (2005)
Biomass burning	Global	GFED2; GFED3.1	1° long. × 1° lat.	van der Werf et al. (2006, 2010) GFED3.1 for CO and GFED2 for others

[*] Before re-gridded to model resolutions.

Table 2. Global budget of tropospheric CO for 2009.

	Global model	Two-way coupled model
Loss by OH reaction ($Tg\,yr^{-1}$)	2364	2400
Transport to stratosphere ($Tg\,yr^{-1}$)	2.8	3.3
Production from methane and NMVOC oxidation ($Tg\,yr^{-1}$)	1465	1497
Emissions ($Tg\,yr^{-1}$)	913[*]	917[*]
Fossil + biofuel	585	589
Biomass burning	328	328
Burden (Tg)	346	383
Tropospheric lifetime (month)	1.75	1.91

[*] The slight difference of $4\,Tg\,yr^{-1}$ (i.e., 913 v.s. 917) is related to the treatment of various offline anthropogenic emission inventories; the effect on CO concentrations is negligible since such a emission difference is less than 0.2 % of total CO sources.

Table 3. Percentage contributions of individual factors to the difference in January 2009 tropospheric CO between the two-way coupled model and the global model, after a 6 month spin-up from July 2008 with consistent initial conditions of chemicals.

Factors	% contribution
All factors	9.6 %
A. Emission magnitude (mainly related to biogenic NMVOC)	3.5 %
B. Nonlinear processes within the troposphere	6.1 %
B1. Small-scale horizontal distributions of NO_x, NMVOC, CO, etc.	4.6 %
B2. Other factors	1.5 %

A. Obtained by contrasting simulations of the global model with vs. without adopting the nested model emissions at individual time steps; emissions are regridded from the nested to coarse resolution.
B. Residual of "All factors" subtracting A.
B1. Residual of B subtracting B2, as driven by small-scale horizontal distributions of emissions resolved on the nested grid but not on the coarse global grid.
B2. Obtained by contrasting simulations of the two-way coupled model with vs. without adopting the global model emissions at individual time steps; emissions are regridded from the coarse to nested resolution, and are thus resolved only at the scale of the coarse grid.

Table 4. Global budget of tropospheric OH for 2009.

	Global model[1]	Two-way coupled model[1]
Total loss (Tg yr^{-1})	3780	3756
OH + CO	1440 (38 %)	1452 (38 %)
OH + CH$_4^2$	540 (14 %)	516 (14 %)
OH + NMVOC	840 (22 %)	852 (23 %)
OH + O$_3$	204 (5 %)	204 (5 %)
OH + HO$_y$	396 (10 %)	384 (10 %)
OH + NO$_y$	72 (2 %)	60 (2 %)
OH + H$_2$, SO$_2$, etc.	132 (9 %)	132 (8 %)
Total production (Tg yr^{-1})	3780	3756
Photolysis of O$_3$	1608 (43 %)	1584 (42 %)
Photolysis of other species	480 (12 %)	504 (14 %)
Reactions	1692 (45 %)	1668 (44 %)
Air mass weighted mean concentration (10^5 cm^{-3})	12.4	11.9
MCF loss rate weighted mean concentration (10^5 cm^{-3})	12.5	12.1
Methyl chloroform lifetime (yr) [3]	5.3	5.5

[1] In the parentheses is the percentage contribution to total loss or production.

[2] In the simulations, the tropospheric mixing ratio of methane (CH$_4$) is fixed at the 2007 level (1732.5 ppb south of 30° S, 1741.7 ppb between 30° S and Equator, 1801.4 ppb between Equator and 30° N, and 1855.6 ppb north of 30° N).

[3] Via the reaction with tropospheric OH, defined as $0.92 \cdot \sum_{i=1}^{T+S} (\Delta P_i \cdot A) / \sum_{i=1}^{T} (\kappa_i \cdot \Delta P_i \cdot C_i \cdot A)$, where i denotes a layer, T the troposphere, S the stratosphere, ΔP_i the delta air pressure, κ_i the reaction constant, C_i the OH concentration, and A the area occupied by a grid cell. The coefficient of 0.92 accounts for the vertical gradient of methyl chloroform mixing ratio (Prather et al., 2012). The horizontal and time dimensions are omitted from the equation for simplicity.

Title Page

Abstract | Introduction

Conclusions | References

Tables | Figures

Back | Close

Full Screen / Esc

Printer-friendly Version

Interactive Discussion

Full Screen / Esc

Printer-friendly Version

Interactive Discussion
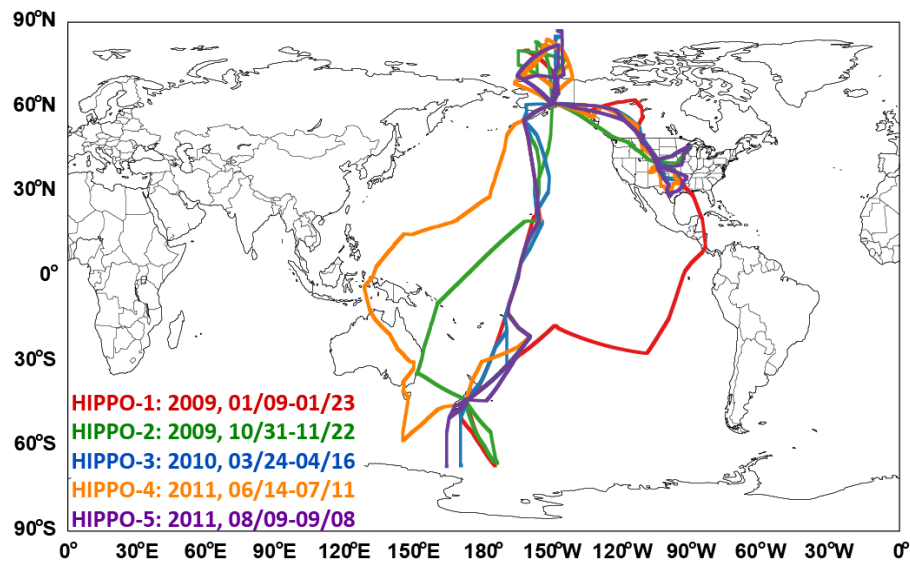
Figure 1. Times and flight tracks of five HIPPO campaigns. Our analysis is focused on CO over the Pacific Ocean.

HIPPO-1: 2009, 01/09-01/23
HIPPO-2: 2009, 10/31-11/22
HIPPO-3: 2010, 03/24-04/16
HIPPO-4: 2011, 06/14-07/11
HIPPO-5: 2011, 08/09-09/08
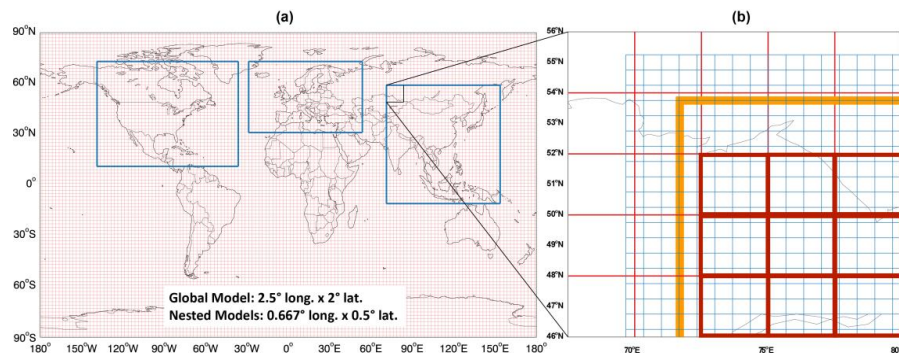
Figure 2. (a) Domains of three nested models covering Asia (70–150° E, 11° S–55° N), North America (140–40° W, 10–70° N) and Europe (30° W–50° E, 30–70° N), respectively. **(b)** Illustration of how global and nested models exchange data in the northwestern corner of the Asian nested domain. Blue denotes nested model grids and red denotes global model grids. Thick yellow lines separate the buffer zone (three outer grid cells) and the inner domain of the nested model. To obtain LBCs, the nested model grid cells in the buffer zone adopt mixing ratios of chemicals from the global model. Global model results in the grid cells fully covered by the inner domain of the nested model (bounded by thickened red lines) are replaced with the nested model results after a mass-conversed regridding process.
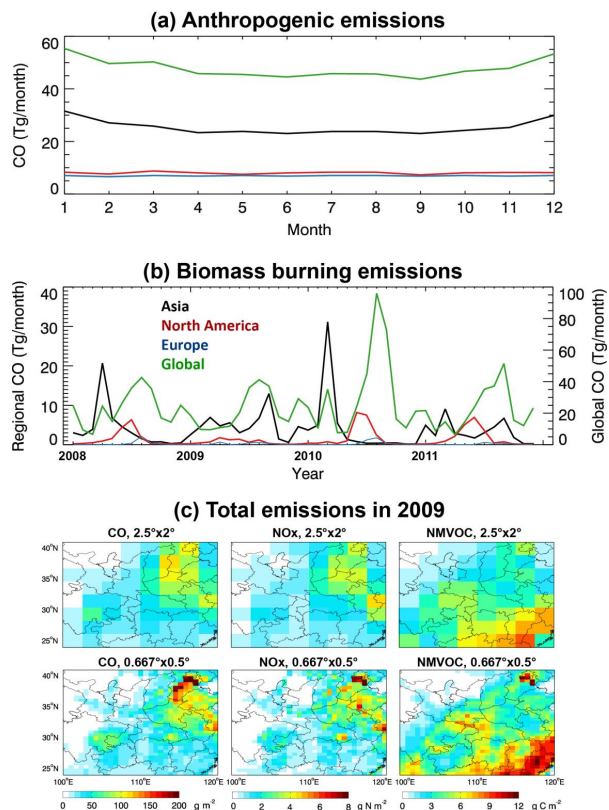
Figure 3. (a) Monthly anthropogenic (fossil + biofuel) emissions of CO within the nested or global model domains; emissions are unchanged from one year to another. **(b)** Monthly biomass burning emissions of CO over 2008–2011 within the nested or global model domains. **(c)** Spatial distributions of CO, NO$_x$ and NMVOC emissions from all sources in 2009 over eastern China on the global vs. nested grids.
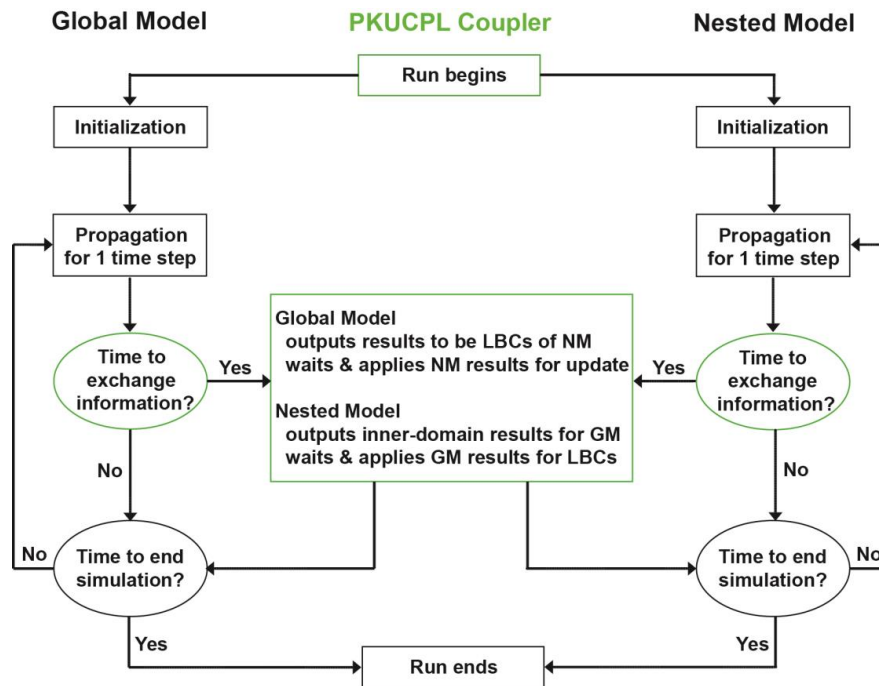
Figure 4. Flowchart of the two-way coupling process. Green indicates the key steps to achieve the two-way integration via the PKUCPL coupler.
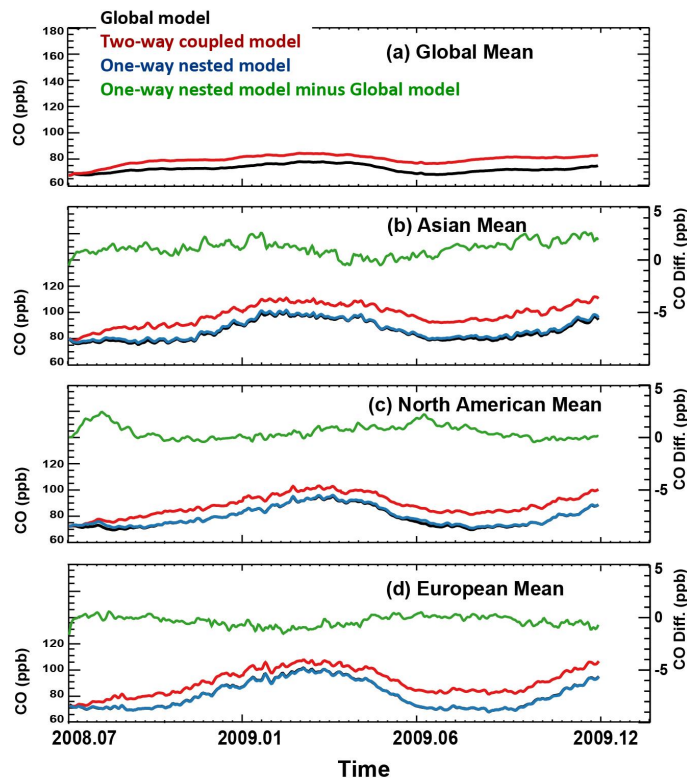
Figure 5. Daily mean tropospheric mean CO mixing ratio from July 2008 through December 2009 averaged over the global or nested model domains simulated by the global model alone (black), by the two-way coupled model (red), and by the one-way nested model (blue; with no feedbacks to the global model; only for nested domains). Also shown in **(b–d)** is the difference between the one-way nested and the global model (green; right axis).
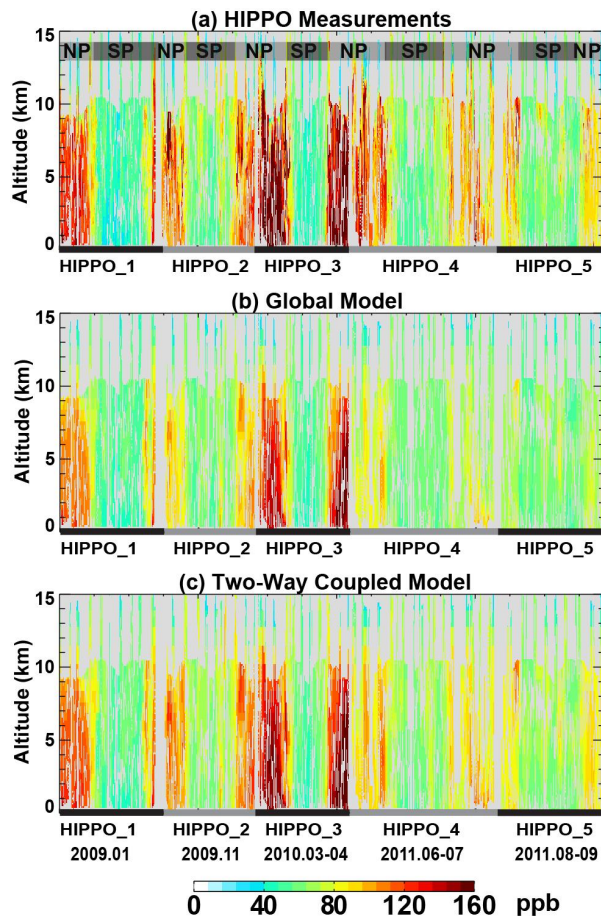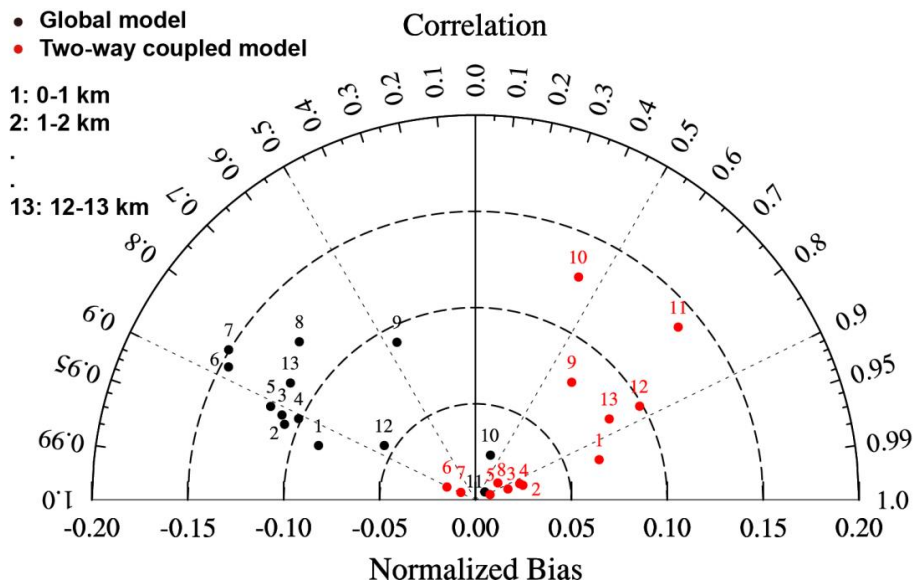
Figure 6. Measured and modeled vertical distributions of tropospheric CO along the flight tracks of HIPPO campaigns. Grey denotes times and locations with no HIPPO data. Data over the North Pacific (NP) and South Pacific (SP) are distinguished in **(a)**.

Figure 7. Correlation and mean normalized bias of modeled CO with respect to HIPPO measurements throughout the HIPPO campaigns, for individual vertical layers (0–1 km, 1–2 km, etc.).
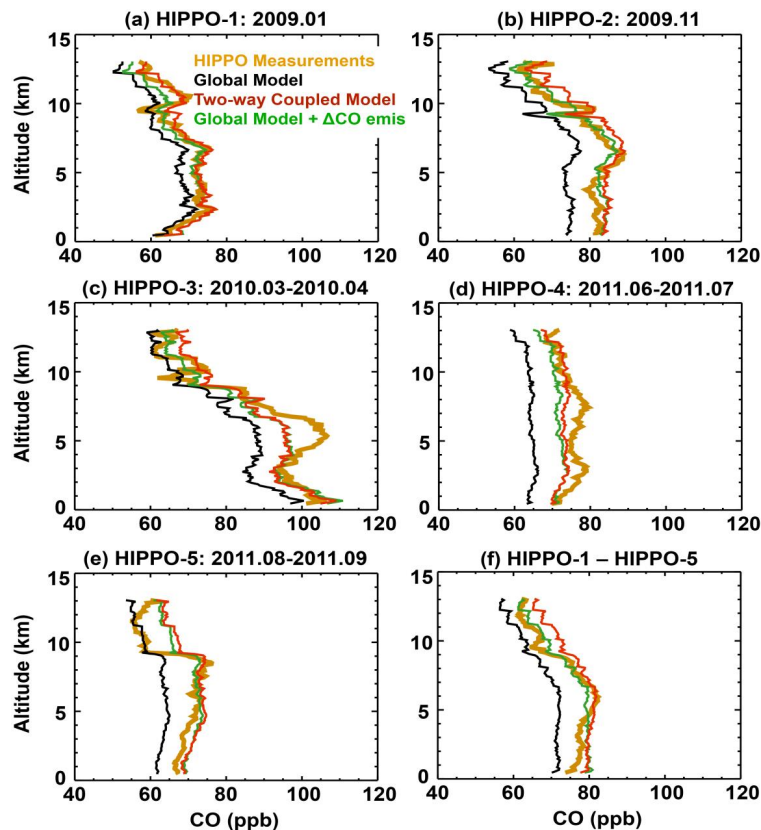
Figure 8. Measured and simulated vertical profiles of CO at 0.1 km intervals averaged over **(a–e)** individual and **(f)** all HIPPO campaigns. Model results are sampled at times and locations coincident to HIPPO measurements. Green lines represent global model simulations with increased global CO emissions that roughly resemble the two-way coupled simulation (especially below 4 km); increases in CO emissions are 15 % for HIPPO-1, 25 % for HIPPO-2, 15 % for HIPPO-3, 25 % for HIPPO-4, and 35 % for HIPPO-5.

Discussion Paper | Discussion Paper | Discussion Paper | Discussion Paper |

ACPD

14, 18961–18996, 2014

Two-way coupled simulation of GEOS-Chem

Y.-Y. Yan et al.

Title Page

Abstract | Introduction

Conclusions | References

Tables | Figures

|◄ | ►|

◄ | ►

Back | Close

Full Screen / Esc

Printer-friendly Version

Interactive Discussion